



# Characteristics of monolithic multisection distributed-Bragg-reflector master-oscillator power-amplifiers

Vasile Tronciu<sup>1</sup> · Eugeniu Grigoriev<sup>1</sup> · Christof Zink<sup>2</sup> · Hans Wenzel<sup>2</sup>

Received: 11 February 2022 / Accepted: 1 July 2022

© The Author(s), under exclusive licence to Springer Science+Business Media, LLC, part of Springer Nature 2022

## Abstract

We report theoretical results on the wavelength stability of a multisection master-oscillator power-amplifier emitting at 1064 nm. We use a traveling wave equation model to calculate the optical output power and spectral maps versus the currents injected into the different sections of the device. The numerical model explains quantitatively the experimental findings, particularly the collapse of the power if the current injected into a control section adjacent to the distributed Bragg reflector laser acting as master oscillator exceeds certain values. We investigate the influence of the reflectivity at the facet of the power amplifier on the laser behavior.

**Keywords** Multisection DBR · MOPA · Bragg grating · Traveling wave model

## 1 Introduction

Applications like free-space communication, spectroscopy, and nonlinear frequency conversion require devices with spatially diffraction-limited and spectrally narrow-band emission at several hundreds of milliwatts or even watts output power (Brox et al. 2008; Jensen et al. 2009; Crump et al. 2012). These requirements can be met by monolithically integrated master-oscillator (MO) power-amplifier (PA) devices where the MO is realized either as a ridge-waveguide (RW) distributed feedback (DFB) laser (Brox et al. 2008; Spreemann et al. 2009; Jedrzejczyk et al. 2010) or distributed-Bragg reflector (DBR) laser (Wenzel et al. 2007; Zink et al. 2020). The MO emits a single lateral and longitudinal lasing mode, which is strongly amplified in the RW (Brox et al. 2008) or tapered amplifiers (Wenzel et al. 2007; Spreemann et al. 2009; Jedrzejczyk et al. 2010; Zink et al. 2020) monolithically integrated with the MO.

---

✉ Vasile Tronciu  
vasile.tronciu@adm.utm.md

<sup>1</sup> Department of Physics, Technical University of Moldova, bd. Stefan cel Mare 168, 2004 Chişinău, Moldova

<sup>2</sup> Ferdinand-Braun-Institut gGmbH, Leibniz-Institut für Höchstfrequenztechnik, Gustav-Kirchhoff-Str. 4, 12489 Berlin, Germany

Typically, the MOPAs have at least two electrically separated contacts, one for the MO and the other for the PA. However, the PA can disturb the MO by thermal cross-talk or optical feedback, resulting in spatio-temporal instabilities such as self pulsations, longitudinal-multi-mode operation, and a deterioration of the spatial beam properties (Mindaugas et al. 2008; Tronciu et al. 2009). In order to decouple MO and PA, an additional section with an electrically separated contact, called preamplifier (Jedrzejczyk et al. 2010) or control section (Zink et al. 2018) can be implemented between MO and PA. However, it was found experimentally that such a control section can result in a lasing collapse (Zink et al. 2018). In this paper, we reveal theoretically the origin of this phenomenon. We also investigate the influence of the reflectivity at the facet of the power amplifier resulting in an unexpected spectral behavior (Zink et al. 2018) which can be avoided by implementing a waveguide tilt at the facet (Zink et al. 2020).

In this paper, we use a time-dependent traveling wave (TW) model taking into account the coupling for forward and backward propagating fields in the Bragg section. In Refs. (Spremann et al. 2009; Mindaugas et al. 2008), and Tronciu et al. (2009) a TW model was used which takes into account both axial ( $z$ ) and lateral ( $x$ ) directions. Due to the fact that the effort for its numerical solution is rather expensive, we use here a simpler model (Radziunas and Wünsche 2005; Radziunas 2017) neglecting lateral field diffraction, treating tapered amplifiers simply as a straight amplifier. It was shown in Ref. (Mindaugas et al. 2008) that such a simplified model suffices to explain the dynamical behavior qualitatively.

The paper is organized as follows. The device structure and experimental results are given in Sect. 2. Then, the TW model is described in Sect. 3. Results of the numerical simulations are presented in Sect. 4. Finally, conclusions are given in Sect. 5.

## 2 MOPA structure and experimental results

As mentioned in the Introduction, the multisection MOPA under study, schematically shown in Fig. 1, is similar to the device reported in Zink et al. (2018). The only difference is that we replaced the tapered PA with a straight one. It was shown in Ref. (Mindaugas et al. 2008) that such a simplification still allows a correct qualitative description. Moreover, we leave the PA section unbiased (current  $I_{PA}$ ) so that it is optically pumped to near transparency. The MOPA consists of 5 sections, namely (from the right- to the left-hand side in Fig. 1): a 1 mm long DBR section at the rear, a 0.75 mm long gain section G, a 0.25 mm long DBR section, a 0.5 mm long preamplifier or control section CON, and a 3.5 mm

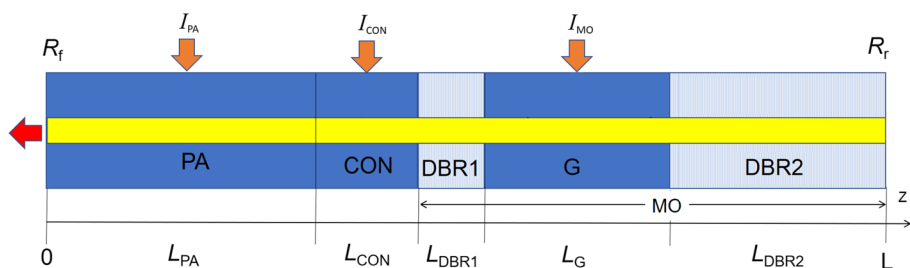


**Fig. 1** Schematic view of DBR MOPA device with indicated currents and lengths of the different sections. Throughout the paper, the current  $I_{PA}$  injected into the power amplifier is set to zero

long PA at the front. The total length of the device is 6 mm. The active layer based on three compressively strained InGaAs quantum wells extends over all sections. The intended lasing wavelength is around 1064 nm. Both facets of the device are anti-reflection coated. In the simulation, we set the reflectivity  $R_r$  at the rear facet (DBR2) to zero and varied the intensity reflectivity at the front facet (PA) from 0 to  $10^{-2}$ .

In what follows, we show for convenience some experimental results already presented in Zink et al. (2018). The power-current characteristic of the MO section measured with a current step of 2 mA is given in Fig. 2a. Note that the emission propagates through the unbiased CON and PA sections where some part of the power is absorbed. Lasing starts at an MO current of  $I_{MO} = 0.1$ A. With increasing MO current, the output power rises nonlinearly with a sawtooth-like shape caused by longitudinal mode jumps as typically observed for DBR lasers (Radziunas et al. 2011; Tronciu et al. 2020). The period of the mode jumps is  $\Delta I_{MO} \approx 0.055$  A just above threshold and decreases with increasing MO current due to dominating Joule heating which is proportional to the injection current squared. In Fig. 2b the power-current characteristics in dependence on the CON current are shown for three different MO currents. The output power increases non-linearly with the CON current up to a maximum value  $I_{CON,MAX}$  depending on the MO current. A further increase of the CON current above  $I_{CON,MAX}$  results in a reduction of the output power until a critical current  $I_{CON,CRI}$  is reached. Above this critical current, no laser emission is observed (lasing collapse). The critical current  $I_{CON,CRI}$  depends on the MO current and the heat sink temperature (not shown here).

### 3 Numerical model and parameters

The numerical model used here is based on the  $1 \times 1$  (time  $\times$  axial position) dimensional traveling wave equations for the slowly varying complex amplitudes  $E^+(z, t)$  and  $E^-(z, t)$  of the counter-propagating optical fields within each section of the device (Radziunas and Wünsche 2005; Radziunas 2017)

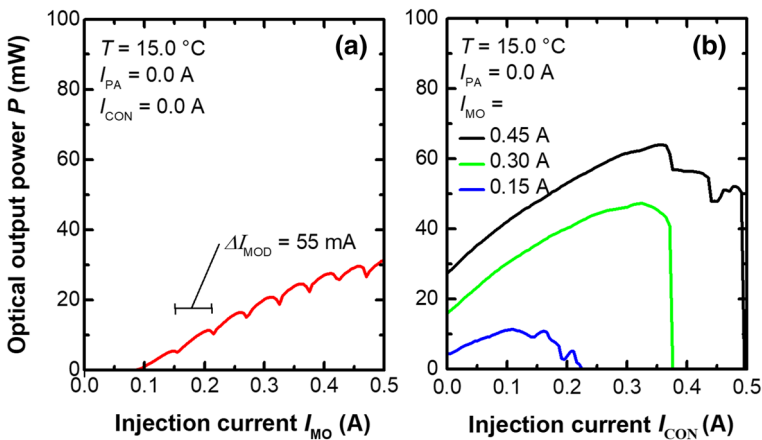


**Fig. 2** Experimental results. **a** Optical output power in dependence on the MO current. PA and CON sections are unbiased. **b** Optical output power in dependence on the CON current

$$\frac{n_g}{c_0} \frac{\partial}{\partial t} E^\pm(z, t) = \left[ \mp \frac{\partial}{\partial z} - i\Delta\beta(N, I) \right] E^\pm(z, t) - i\kappa E^\mp(z, t) + F_{\text{sp}}^\pm \quad (1)$$

where  $c_0$  is the speed of light in vacuum,  $F_{\text{sp}}^\pm$  the stochastic contribution of the spontaneous emission,  $n_g$  the group index, and  $\kappa$  the field coupling coefficient due to Bragg gratings. The relative propagation factor in each section is given by

$$\Delta\beta = \delta_0 - i\frac{\alpha_0}{2} + k_0 [\Delta n_N(N) + \Delta n_T(I)] + i\frac{g(N) - \mathcal{D}}{2}, \quad (2)$$

where  $\delta_0$  is a static detuning between the sections due to different modal refractive indices,  $\alpha_0$  the internal optical losses,  $k_0 = 2\pi/\lambda_0$  with  $\lambda_0$  being the reference wavelength, and  $\mathcal{D}$  a linear operator modeling gain dispersion. The modal peak gain is assumed to depend logarithmically on the carrier density,

$$g(N) = \Gamma g' N_{\text{tr}} \ln \left( \frac{N}{N_{\text{tr}}} \right) \quad (3)$$

where  $\Gamma$  is the optical confinement factor,  $g'$  the differential gain, and  $N_{\text{tr}}$  the transparency carrier density. The change of the modal index with carrier density is modeled by the square root function (Spremann et al. 2009)

$$\Delta n_N = \tilde{\alpha}_H \frac{\Gamma g' N_{\text{tr}}}{k_0} \sqrt{\frac{N}{N_{\text{tr}}}}. \quad (4)$$

The function  $\Delta n_T(I)$  describes the change of the modal index in a laser section  $k$  due to self and cross heating induced by the currents injected in sections  $r$  (Spremann et al. 2009; Radziunas et al. 2011),

$$\Delta n_{T,k} = \frac{n_g}{\lambda_0} \sum_r C_k^r \cdot I_r, \quad r, k \in [PA, CON, DBR1, G, DBR2], \quad (5)$$

being the major factor implying transitions between longitudinal modes when the injection current is varied. We mention that in our calculations we consider only the changes of the modal indices induced by currents injected into adjacent sections. In this paper, we assume the following values for the self-heating and cross-heating coefficients:  $C_{\text{PA}}^{\text{PA}} = 0.05$  nm/A,  $C_{\text{CON}}^{\text{CON}} = 6.0$  nm/A,  $C_G^G = 4.0$  nm/A,  $C_{\text{CON}}^{\text{PA}} = C_{\text{PA}}^{\text{CON}} = C_{\text{DBR1}}^G = C_{\text{DBR2}}^G = 0.35$  nm/A,  $C_{\text{DBR1}}^{\text{CON}} = 1.0$  nm/A. Note, that we neglected any longitudinal variation of the self and cross heating in each section.

The rate equation for the carrier density  $N(z, t)$  in each section reads

$$\begin{aligned} \frac{\partial}{\partial t} N = & \frac{I_k}{edWL_k} + \frac{U_F'}{edWL_k r_s} (\bar{N} - N) - (AN + BN^2 + CN^3) \\ & - \frac{c_0}{n_g} \Re \sum_{\nu=\pm} E^{\nu*} [g(N) - \mathcal{D}] E^\nu, \end{aligned} \quad (6)$$

where  $I_k$  is the current injected into section  $k$  with length  $L_k$ ,  $e$  is the elementary charge,  $d$  and  $W$  are thickness and width, respectively, of the active region, and  $A$ ,  $B$  and  $C$  are the recombination parameters. The second term on the right hand side describes the self-distribution of the injected current due to a non-vanishing area-related series resistance  $r_s$  with

$U'_F$  being the derivative of the Fermi level separation and  $\bar{N}$  is the average carrier density in the section. The last term in (6) is the rate of stimulated recombination where  $\Re$  means ‘real part’. For a detailed description of the remaining model equations and parameters, we refer to Radziunas and Wünsche (2005) and Radziunas (2017). The values of main laser parameters used in our simulations are collected in Table 1.

### 4 Results and discussions

In this section, we present the numerical results obtained using the TW model (1)-(6) incorporated in the software LDSL and the parameters given in Table 1. We start our simulations by finding the properties of the MO. With this in mind, the currents injected into CON and PA sections are kept constant equals zero. Figure 3a shows the dependence of the optical output power at the front facet (at the PA) versus the current injected into the gain section of the MO. The threshold current is 0.1 A, similar to the one obtained in the experiment (see Fig. 2a). When the MO current is increased, the output power rises with the typical sawtooth like shape caused by the longitudinal mode jumps as already discussed (see Fig. 3b). The current period of the mode jumps is  $\Delta I_{MO} \approx 53$  mA, similarly as observed in the experiment (Fig. 2).

**Table 1** Parameters of the standard configuration

Symbol	Description	Unit	Value
$\lambda_0$	Reference wavelength	m	$1.06 \times 10^{-6}$
$L_G$	Length of active section	m	$0.75 \times 10^{-3}$
$L_{DBR1}$	Length of DBR section	m	$0.25 \times 10^{-3}$
$L_{DBR2}$	Length of DBR section	m	$1.0 \times 10^{-3}$
$L_{CON}$	Length of CON section	m	$0.5 \times 10^{-3}$
$L_{PA}$	Length of PA section	m	$3.5 \times 10^{-3}$
$R_r$	Rear facet intensity reflectivity		0
$R_f$	Front facet intensity reflectivity		0 ... 0.01
$n_g$	Group refractive index		3.7
$\kappa$	Coupling coefficient	$m^{-1}$	$10 \times 10^2$
$\alpha_H$	Linewidth enhancement factor		-2.0
$\alpha_0$	Internal absorption	$m^{-1}$	$2 \times 10^2$
$\Gamma$	Optical confinement factor		$2.2 \times 10^{-2}$
$g'$	Differential gain	$m^2$	$1450 \times 10^{-22}$
$c_g$	Gain compression factor	$m^3$	$1 \times 10^{-24}$
$N_{tr}$	Transparency carrier density	$m^{-1}$	$1.2 \times 10^{-24}$
$d$	Thickness of active layer	m	$7 \times 10^{-9}$
$W$	Width of active layer	m	$8 \times 10^{-6}$
$r_s$	Series resistance	$\Omega m^2$	$0.5 \times 10^{-8}$
$A$	Recombination parameter	$s^{-1}$	$1.7 \times 10^{-9}$
$B$	Recombination parameter	$m^3 s^{-1}$	$1 \times 10^{-16}$
$C$	Recombination parameter	$m^6 s^{-1}$	$40 \times 10^{-42}$
$U'_F$	Derivative of Fermi level separation	$V m^3$	$0.04 \times 10^{-24}$

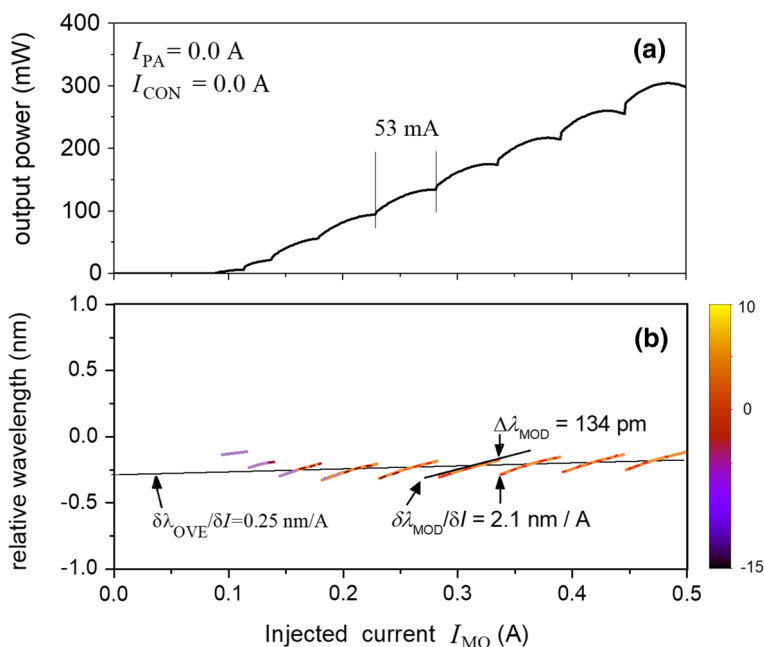
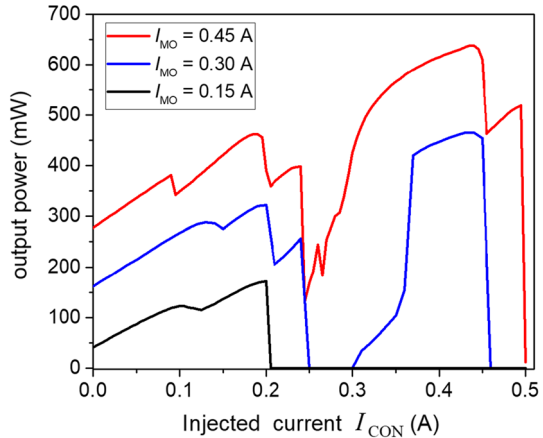


**Fig. 3** **a** Calculated output power versus current injected into the gain section G of the MO. **b** Pseudo-color mapping of the optical spectral densities (in dB) as a function of the MO current and the wavelength relative to the reference wavelength (the noisy background is white). The PA and CON sections are unbiased, i.e. the PA and CON currents equal zero. Front facet reflectivity is zero

Figure 3b shows a mapping of the optical spectra versus the same range of injection currents as in Fig. 3a. The nearly periodic jumps from a longer wavelength mode to a shorter wavelength mode ( $\Delta\lambda_{\text{MOD}} \approx 0.134$  nm) lead to the modulation of the optical power seen in Fig. 3a. Besides the mode jumps, there is also a variation of the overall lasing wavelength, which is mainly determined by the peak of the reflectivity of the DBR section. Just above threshold, the overall wavelength decreases caused by the optical generation of charged carriers in the DBR section resulting in a decrease of the modal index. For larger currents, the heating of the DBR section (given by the parameters  $C_{\text{DBR1}}^{\text{G}} = C_{\text{DBR2}}^{\text{G}}$ ) dominates resulting in a shift of the overall wavelength to larger values. The corresponding slope between 0.3 A and 0.5 A is  $\delta\lambda_{\text{OVE}}/\delta I = 0.25$  nm/A. Within a period between the mode jumps, the wavelength of each mode increases with rising current determined by  $C_{\text{G}}^{\text{G}}$ . For a current of  $I_{\text{MO}} = 0.3$  A, the corresponding slope is  $\delta\lambda_{\text{MOD}}/\delta I = 2.1$  nm/A determined from a linear fit. These values of the slopes as well as the spacing of the longitudinal modes (given by  $\Delta\lambda_{\text{MOD}}$ ) are similar to those of Ref. (Zink et al. 2018).

As mentioned above, until now the PA and CON sections were unbiased. In what follows we consider what happens if the current injected into CON section, i.e. the pre-amplifier current, is varied, still keeping PA unbiased. One would expect that the output power rises linearly with the CON current for sufficiently large input power from the MO, as appropriate for an amplifier in the saturation regime. However, this is only the case for small value of  $I_{\text{CON}}$ . The black line in Fig. 4 shows the dependence of the power on the CON current for a fixed MO current of 0.15 A. The output power rises from

**Fig. 4** Output power versus current injected into the control section for different MO currents as indicated in the legend. Other parameters are as in Fig. 3. Front facet reflectivity is zero. (Color figure online)



45 mW to a maximum value of 170 mW for a CON current of 0.2 A and exhibits a kink at  $I_{CON} \approx 0.11$  A. A further increase of the CON current beyond 0.2 A leads to a drop of the power. No more laser emission is observed (lasing collapse), similarly as in the experiment (Fig. 2). For  $I_{MO} = 0.3$  A an analogous behavior can be stated, but between CON currents of 0.3 A and 0.45 A again lasing operation occurs (blue line of Fig. 4). The output power starts to increase from 160 mW at zero injected CON current and reaches a maximum value of 460 mW for  $I_{CON} = 0.44$  A. For an MO current of 0.45 A the output power rises from 280 mW followed by jumps and nonlinearities up to a maximum power of 640 mW at a CON current of 0.45 A (red line in Fig. 4). The output power drops to zero at a CON current of 0.5 A.

Figure 5 shows a mapping of the optical spectra in dependence on the CON current for the same MO currents as in Fig. 4. For an MO current of 0.15 A, a single jump to a longer wavelength mode occurs at a CON current of 0.125 A. For MO current of 0.3 A, the spectra show different jumps to longer and shorter wavelength modes. One can also see the non-lasing region where no lasing modes, but only noise background (white) exists. For all CON currents, single-mode operation can be observed. If the MO current is further increased to 0.45 A, an additional multi-mode region around 0.25 A appears (see region D in Fig. 5c). This is confirmed by the optical spectrum shown in Fig. 6d.

To understand the modal behavior, we calculated the reflection spectra of sections DBR1 and DBR2 seen from the gain section G for fixed CON currents corresponding to regions A-E in Fig. 5c. The results are shown in Fig. 6 together with the optical spectra for each region. In the simulation, we modeled the heating of DBR1 due to the CON current by the parameter  $C_{DBR1}^{CON} = 1.0$  nm/A, but neglected the corresponding heating of DBR2 ( $C_{DBR2}^{CON} = 0$ ). This model takes into account the effect that in the experiment, the adjacent DBR1 is stronger heated by the current injected into the CON section than the distant DBR2. The heating of DBR1 results in a detuning of the reflection spectra of DBR1 and DBR2 with increasing CON current which is the root cause of the modal behavior. If DBR1 is heated too strongly by a high CON current, the reflection peaks of DBR1 and DBR2 are too far away from each other so that the threshold gain becomes too high and lasing collapse occurs.

Let us study regions A-E in more detail. In region A (Fig. 6a), the lasing mode is located on the left-hand side of the reflection peak of DBR2. An increase of CON current leads to

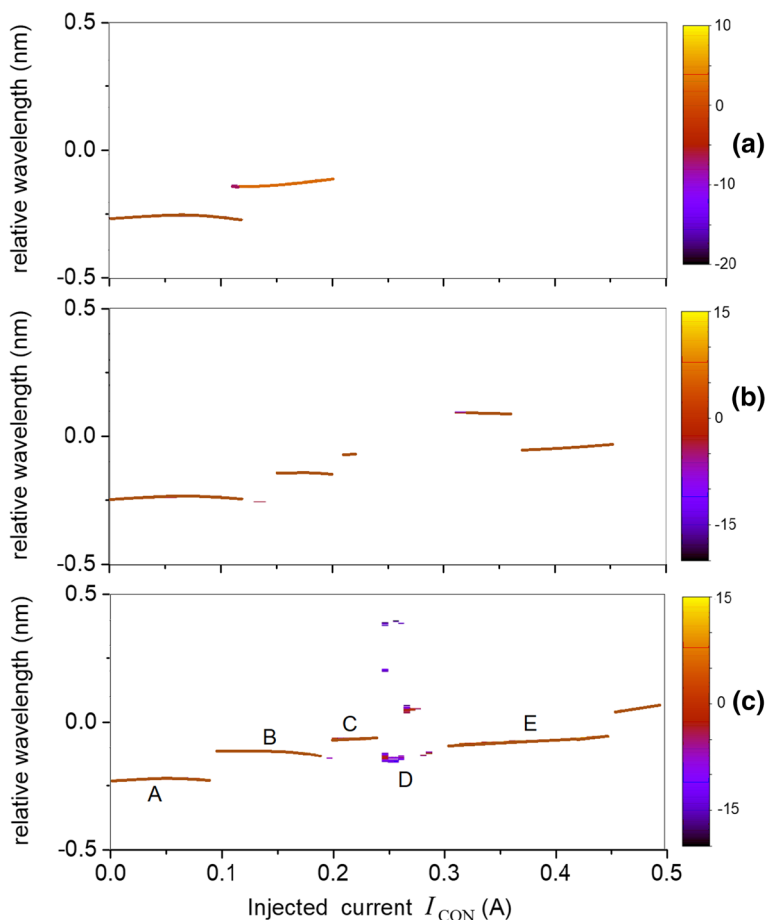


**Fig. 5** Pseudo-color mappings of the optical spectral densities (in dB) as a function of the current injected into the CON section and the wavelength relative to the reference wavelength for the same parameters and MO currents as in as in Fig. 4. **a**  $I_{MO} = 0.15$  A, **b**  $I_{MO} = 0.30$  A, **c**  $I_{MO} = 0.45$  A. The noisy background is white

jumps to longer wavelength modes (regions B and C) on the right-hand side of the reflection peak. The region D is characterized by multi-mode operation because the reflection peaks of DBR1 and DBR2 are too distant from each other, causing strong mode competition. Finally, in region E, the mode jumps back to a shorter-wavelength side peak of the reflection spectrum of DBR1.

In what follows, we study the influence of the front facet reflectivity on the output characteristics of the MOPA. We mention that the reflectivity of the front facet can be affected by employing an appropriate coating or tilting of the lateral waveguide. First, we reproduce in Fig. 7a the dependence of the output power on the CON current for an MO current of 0.45 A and a vanishing reflectivity of the front facet. We plot in this figure like in the following figures the mean (red curve), maximum (blue), and minimum (black) values of the output power collected from pulse traces with a length of 10 ns at the front facet of the device. If these values calculated for each current coincide, the power can be considered

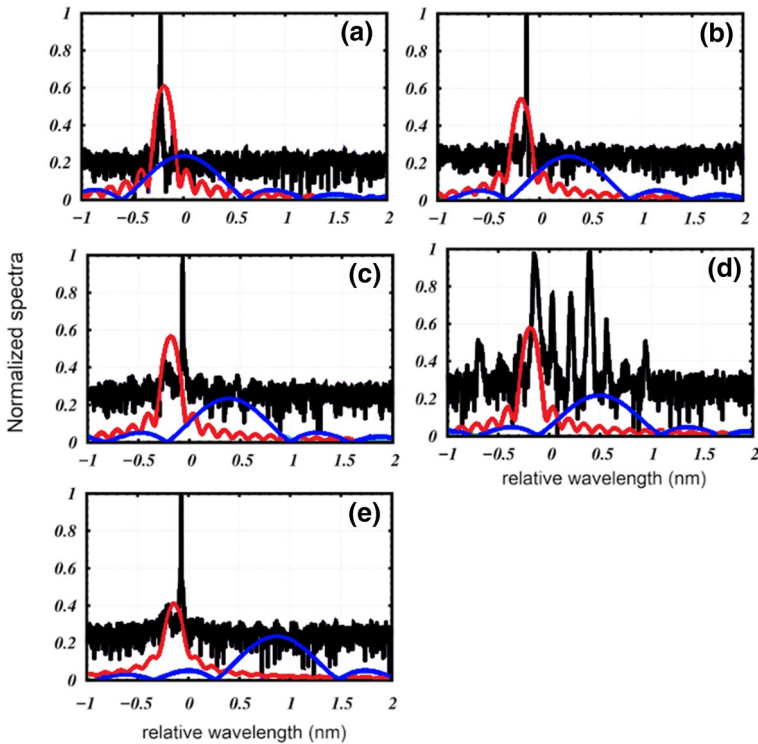


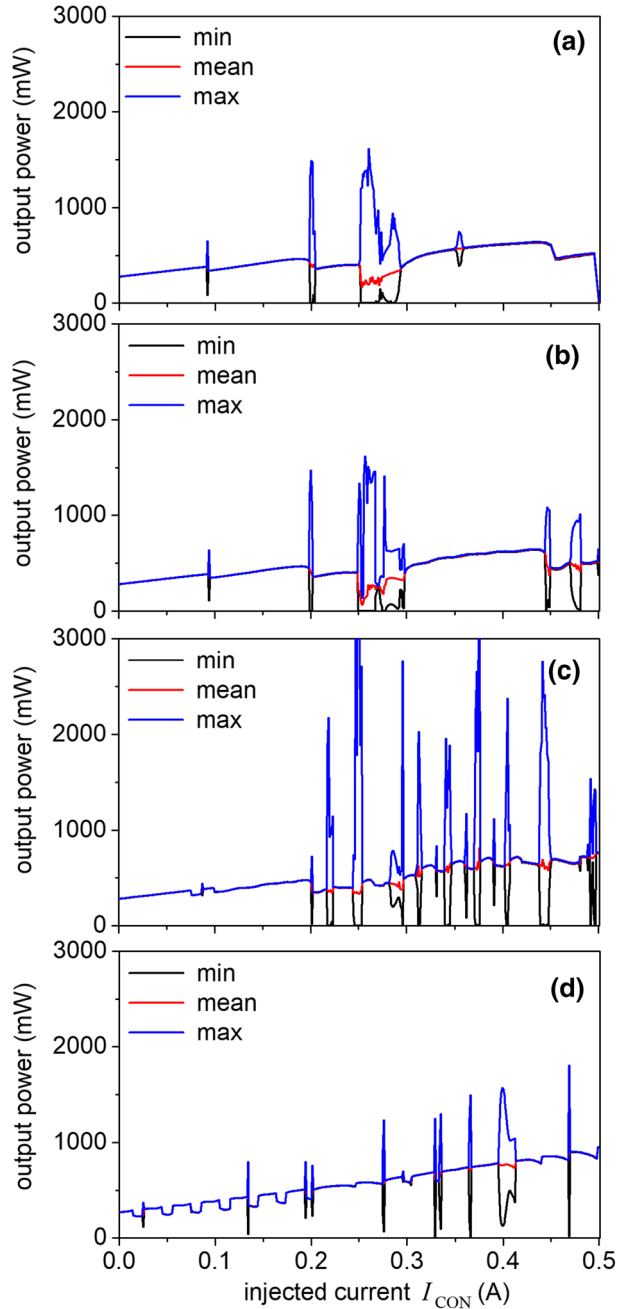
**Fig. 6** Optical spectra (black lines) and reflection spectra of DBR1 (blue) and DBR2 (red) for the different regions of Fig. 5c. (Color figure online)

as temporally constant. Otherwise, the laser exhibits dynamic instabilities, as can be seen between mode jumps or for CON currents between 0.25 and 0.3 A (multi-mode behavior in region D of Fig. 5c). When the front facet reflectivity is increased to  $10^{-6}$  and  $10^{-4}$ , more and more regions of instabilities appear (see Fig. 7b, c). The reason is that in dependence on the current the compound cavity modes lose their stability because of the nonvanishing linewidth enhancement factor coupling phase and amplitude fluctuations (Tromborg et al. 1984). For the highest reflectivity of  $10^{-2}$ , the device exhibits again a more stable behavior. In this case, the whole device can be considered to be a multi-section laser and not a MOPA subject to weak feedback because the cavity is now formed by DBR2 at the rear side and the front facet.

### 5 Summary and conclusions

We presented numerical investigations of the behavior of monolithic DBR MOPAs using a traveling wave model adapted to the specific multi-section device. We were able to reproduce and to explain the experimentally observed non-linear dependence of the optical power on a preamplifier or control current. The root cause of the lasing collapse is a thermal mismatch of both DBR sections resulting in a detuning of the corresponding reflection spectra. In order to prevent the lasing collapse, the control current should be chosen

**Fig. 7** Output power versus current injected into the control section CON for **a**  $R_f = 0.0$ , **b**  $R_f = 10^{-6}$ , **c**  $R_f = 10^{-4}$ , **d**  $R_f = 10^{-2}$ . Other parameters  $I_{MO} = 0.45$  A,  $I_{PA} = 0$



as small as possible (in the ideal case equals zero). Another possibility is a heating of the opposite DBR with micro heaters to compensate the temperature difference. The numerical simulations show a transition between MOPA and laser types of operation if the front facet reflectivity is increased. For a stable MOPA operation, a front facet reflectivity of  $10^{-6}$  or

less is needed, which could be achieved by a tilted PA. We believe that our work provides a good basis for more detailed investigations of stable operating DBR MOPA devices.

**Acknowledgements** Part of this work was supported by the National Agency for Research and Development of Moldova within the project 20.80009.5007.08 “Study of optoelectronic structures and thermoelectric devices with high efficiency”. We are indebted to M.Radziunas (WIAS Berlin) for his support in using the LDSL tool.

**Funding** The authors have not disclosed any funding.

## Declarations

**Conflict of interest** The authors have not disclosed any conflict of interest.

## References

- A software package LDSL-tool. Longitudinal Dynamics of multisection Semiconductor Lasers. <http://www.wias-berlin.de/software/ldsl>
- Brox, O., Wiedmann, J., Scholz, F., Bugge, F., Fricke, J., Klehr, A., Laurent, T., Ressel, P., Wenzel, H., Erbert, G., Tränkle, G.: Integrated 1060nm MOPA pump source for high-power green light emitters in display technology. *Proc. SPIE* **6909**, 69091G (2008)
- Crump, P., Brox, O., Bugge, F., Fricke, J., Schultz, C., Spreemann, M., Sumpf, B., Wenzel, H., Erbert, G.: High power, high efficiency monolithic edge-emitting GaAs-based lasers with narrow spectral widths. In: Coleman, J.J., Bryce, A.C., Jagdish, C. (eds.) *Advances in Semiconductor Lasers*, pp. 49–91. Academic Press (2012)
- Jedrzejczyk, D., Brox, O., Bugge, F., Fricke, G., Ginolas, A., Paschke, K., Wenzel, H., Erbert, G.: High-power distributed-feedback tapered master-oscillator power amplifiers emitting at 1064 nm. *Proc. SPIE* **7583**, 758317 (2010)
- Jensen, O.B., Andersen, P.E., Sumpf, B., Hasler, K.H., Erbert, G., Petersen, P.M.: 1.5 W green light generation by single-pass second harmonic generation of a single-frequency tapered diode laser. *Opt. Express* **17**(8), 6532–6539 (2009)
- Mindaugas, R., Tronciu, V., Bandelow, U., Lichtner, M., Spreemann, M., Wenzel, H.: Mode transitions in distributed-feedback tapered master-oscillator power-amplifier: theory and experiments. *Opt. Quant. Electron.* **40**, 1103–1109 (2008)
- Radziunas, M.: traveling wave modeling of nonlinear dynamics in multisection laser diodes. In: Piprek, J. (ed.) *Handbook of Optoelectronic Device Modeling and Simulation Lasers, Modulators, Photodetectors, Solar Cells, and Numerical Methods*, CRC press. (2017)
- Radziunas, M., Wünsche, H.J.: Multisection lasers: longitudinal modes and their dynamics. In: Piprek, J. (ed.) *Optoelectron Devices*, pp. 121–150. Springer, New York (2005)
- Radziunas, M., Hasler, K.H., Sumpf, B., Tien, T.Q., Wenzel, H.: Mode transitions in distributed bragg reflector semiconductor lasers: experiments, simulations and analysis. *J. Phys. B: Atomic Mol. Opt. Phys.* **44**(10), 105401 (2011)
- Spreemann, M., Lichtner, M., Radziunas, M., Bandelow, U., Wenzel, H.: Measurement and simulation of distributed-feedback tapered master-oscillator power amplifiers. *IEEE J. Quant. Electron.* **45**(6), 609–616 (2009)
- Tromborg, B., Osmundsen, J., Olesen, H.: Stability analysis for a semiconductor laser in an external cavity. *IEEE J. Quant. Electron.* **20**, 1023–1032 (1984)
- Tronciu, V., Lichtner, M., Radziunas, M., Bandelow, U., Wenzel, H.: Improving the stability of distributed-feedback tapered master-oscillator power-amplifiers. *Opt. Quant. Electron.* **41**, 531–537 (2009)
- Tronciu, V., Wenzel, H., Radziunas, M., Reggentin, M., Wiedmann, J., Knigge, A.: Investigation of red-emitting distributed Bragg reflector lasers by means of numerical simulations. *IET Optoelectron.* **12**, 228–232 (2020)

- Wenzel, H., Paschke, K., Brox, O., Bugge, F., Fricke, J., Ginolas, A., Knauer, A., Ressel, P., Erbert, G.: 10 W continuous-wave monolithically integrated master-oscillator power-amplifier. *Electron. Lett.* **43**, 160–161 (2007)
- Zink, C., Maaßdorf, A., Fricke, J., Ressel, P., Maiwald, M., Sumpf, B., Erbert, G., Tränkle, G.: Diffraction limited 1064 nm monolithic DBR-master oscillator power amplifier with more than 7 W output power. *Proc. SPIE* **10553**, 105531C (2018)
- Zink, C., Maaßdorf, A., Fricke, J., Ressel, P., Sumpf, B., Erbert, G., Tränkle, G.: Monolithic master oscillator tilted tapered power amplifier emitting 9.5 W at 1060 nm. *IEEE Photon. Technol. Lett.* **32**, 59 (2020)

**Publisher's Note** Springer Nature remains neutral with regard to jurisdictional claims in published maps and institutional affiliations.